Online Adaptation of Performance Maps for Centrifugal Gas Compressors

Andrea Cortinovis, Matteo Zovadelli, Mehmet Mercangöz, Diego Pareschi,
Antonio De Marco and Sergio Bittanti

***Abstract*— This paper investigates the adaptation of different performance maps of centrifugal compressors driven by dual-shaft gas turbines during operation. First the estimation of compressor, gas turbine and combined efficiency are considered. Obtaining performance maps is mainly based on fitting an empirical model to the history of past data together with the understanding of how much new information is contained in newly collected data samples. This amounts to solving a least-squares problem which is formulated as a quadratic program using various constraints. Comparing the actual efficiency to the predicted efficiency by evaluating the previously fitted model, the algorithm decides whether the actual model is accurate enough or a model update is needed. The necessity of having an online model update comes from the fact that the efficiency maps can change due to several factors such as fouling. The algorithm is tested using industrial data from a gas compression station with five gas turbine-driven compressors. The results show the need of online adaptation and that it is possible to accurately predict the different efficiencies using the presented method without excessive model updates. The access to online updated performance maps allows to understand how well the system is performing and gives the opportunity to monitor the efficiency of a specific unit. It is possible to use the adapted performance maps for load sharing optimization with time-varying optimization models.**

I. Introduction

The purpose of compressor stations along pipelines is to pump a quantity of natural gas at a desired pressure level. A compressor station consists of several compressor trains connected in series, parallel or mixed configurations. The analysis of turbo compressors indicates that the energy consumption takes up to 70% of the cost [1]. The major innovation in the past decade was the trend going from fixed-speed drivers to variable-speed dual-shaft gas turbines and variable-speed electrical drives. By using variable-speed driven compressors, manufacturers have enlarged the operating range and the flexibility. This change led to more efficient operation, but also increased the control complexity of compression stations. For example, using the conventional load sharing approach of equal set points for all variable-speed compressor units typically leads to inefficient operation and poor exploitation of the gained operational flexibility [2]. The total energy consumption can therefore be additionally reduced by optimizing the operation of compressor stations. This will significantly impact the overall operation and maintenance costs of a gas compression station. These considerations point out that advanced load sharing optimization is very promising but the lack of information on the performance map of the individual compressors, which are needed to optimize the system stands as an obstacle for the implementation of such schemes. The performance map of a compressor is subject to significant changes caused by external and unknown factors [3]. Therefore, it is important for load sharing optimization to have an efficiency model, whose performance is monitored and whose parameters are up-to-date [4].

Typically the compressor map (relationship between head and flow at varying speeds) and performance map (efficiency at varying operating points) are tested periodically but to a very limited extent to minimize down-time and the corresponding economic loss. Due to the infrequent nature of these tests, it is rather common to have invalid or inaccurate information on the compressor and performance maps. This lack of information makes it particularly difficult to optimize the compression system for load sharing [5].

In the present paper the thermodynamic modeling and estimation of various efficiencies related to the operation of gas turbine driven compressors are discussed. An adaptation algorithm is used to fit historical data to a specific empirical model resulting in a compressor map. The advantage of this method compared to pure black box modeling [6] is that it provides flexibility to explicitly specify the form of the compressor map. This map can be evaluated for different operating points to obtain a predicted efficiency of the compressor. By comparing the efficiency obtained from measurements and thermodynamic relationships with the predicted efficiency, the accuracy of the performance map can be determined. In the case of large deviations the method is able to update the model parameters of the performance map in order to improve the accuracy of the predictions. This requires a trade-off between overfitting and underfitting the model to the considered history of data points.

The results are obtained using industrial data from a five compressor station with centrifugal compressors driven by dual-shaft gas turbines. The arrangement considered in this study is depicted in Fig. 1. The first shaft connects air compressor and high pressure turbine (HPT) of the gas turbine, whereas the second shaft connects the low pressure turbine (LPT) to the gas compressor used to compress the process gas. This arrangement ensures that the speeds of the two shafts can be chosen independently. The presented

A. Cortinovis and M. Mercangöz are with ABB Switzerland Ltd., Corporate Research Center, Baden Dättwill, AG 5405 Switzerland (e-mail: andrea.cortinovis@ch.abb.com, mehmet.mercangoez@ch.abb.com)

M. Zovadelli, A. De Marco and S. Bittanti are with the Politecnico di Milano - DEIB, Via Ponzio, 34/5, Milano, 20133 Italy (e-mail: sergio.bittanti@polimi.it, matteo.zovadelli@gmail.com)

D. Pareschi is with ABB Spa, Process Automation Division, Oil Gas and Petrochemicals BU, Via L. Lama 33, Sesto San Giovanni, Milano, 20099 Italy, (e-mail: diego.pareschi@it.abb.com)

method is not restricted to this kind of arrangement and can easily be extended to electrical driven gas compressors.

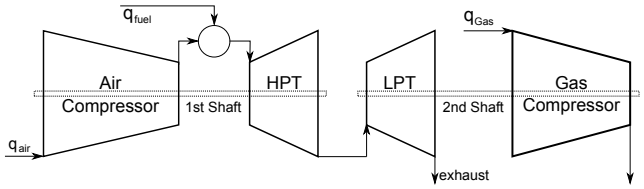

Fig. 1. Typical variable speed dual-shaft gas turbine and centrifugal gas compressor

II. Setup and Statistical Data Analysis

This section presents the considered setup and discusses the statistical correlation between the different measured variables. Data was collected during one year, with a sampling rate of one hour at a compression plant with five gas turbine-driven compressors. The data contains most of the possible variations of ambient conditions, operating conditions and equipment deterioration. The available measurements for each individual compressor are listed in the following and illustrated in Fig. 2.

- Suction pressure p_s and discharge pressure p_d in $[barg]$
- Suction temperature T_s and discharge temperature T_d in $[^\circ C]$
- Suction flow q_s in [compensated m^3/h]
- Fuel flow q_f in [compensated m^3/h]
- Compressor speed Ω in $[rpm]$

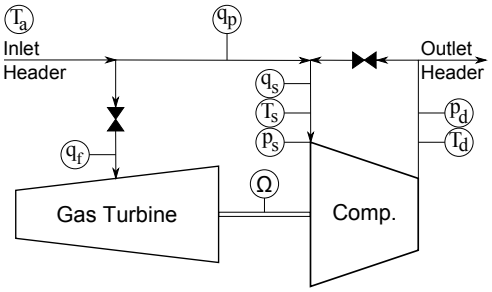

Fig. 2. Simplified system with available measured variables

Note that volumetric flows q_s and q_f can easily be converted to mass flows $\dot{m}_s$ and $\dot{m}_f$ by using the density of natural gas ρ_0 at standard conditions. The ambient temperature T_a is measured for the station and is the same for all compressor units. It has to be noted that for pipeline applications the gas composition is well known unlike for example upstream operations where the gas composition can change over a short period of time.

The correlation of measured variables is a valuable information to understand which variables might influence the calculated efficiencies and to which extent. For this reason, the collected data was processed in an off-line fashion by calculating the measurement covariance matrix which is defined in Eq. 1.

$$\Sigma_{ij} = E[(X_i - \mu_i) \cdot (X_j - \mu_j)] \tag{1}$$

with the mean values $\mu_i = E[X_i]$. The measurement covariance matrix Σ depends on the window length of the considered data and may vary for different seasons. Therefore, the correlation is shown for a short time interval of two weeks corresponding to 336 data points in summer and in winter. This ensures that the overall conditions are similar in the considered time interval. The measurement covariance matrices for the two selected cases are shown in Tab. I and Tab. II. The covariance matrices have been

	q_s	q_f	p_s	p_d	Π	T_s	T_d	Ω	T_a	η_{iso}	η_{gt}	η_{tot}	
q_s	1	0.87	-0.05	-0.21	-0.15	0.03	0.42	0.74	-0.12	0.05	0.16	0.07	q_s
q_f	0.87	1	-0.43	-0.09	0.30	-0.17	0.74	0.96	-0.08	0.29	0.40	0.32	q_f
p_s	-0.05	-0.43	1	0.39	-0.57	0.66	-0.42	-0.64	-0.16	-0.17	-0.23	-0.20	p_s
p_d	-0.21	-0.09	0.39	1	0.54	0.21	0.34	-0.19	-0.03	0.56	0.50	0.56	p_d
Π	-0.15	0.30	-0.57	0.54	1	-0.43	0.68	0.41	0.12	0.65	0.65	0.68	Π
T_s	0.03	-0.17	0.66	0.21	-0.43	1	0.09	-0.27	-0.19	-0.13	-0.16	-0.15	T_s
T_d	0.42	0.74	-0.42	0.34	0.68	0.09	1	0.78	-0.04	0.56	0.62	0.59	T_d
Ω	0.74	0.96	-0.64	-0.19	0.41	-0.27	0.78	1	-0.02	0.30	0.42	0.34	Ω
T_a	-0.12	-0.08	-0.16	-0.03	0.12	-0.19	-0.04	-0.02	1	0.15	0.14	0.15	T_a
η_{iso}	0.05	0.29	-0.17	0.56	0.65	-0.13	0.56	0.30	0.15	1	0.99	1	η_{iso}
η_{gt}	0.16	0.40	-0.23	0.50	0.65	-0.16	0.62	0.42	0.14	0.99	1	0.99	η_{gt}
η_{tot}	0.07	0.32	-0.20	0.56	0.68	-0.15	0.59	0.34	0.15	1	0.99	1	η_{tot}

TABLE I

Summer correlation matrix

	q_s	q_f	p_s	p_d	Π	T_s	T_d	Ω	T_a	η_{iso}	η_{gt}	η_{tot}	
q_s	1	0.89	-0.08	0.53	0.39	-0.39	0.61	0.82	-0.07	0.47	0.56	0.51	q_s
q_f	0.89	1	-0.46	0.77	0.73	-0.40	0.88	0.98	-0.16	0.70	0.77	0.74	q_f
p_s	-0.08	-0.46	1	-0.53	-0.81	0.24	-0.72	-0.57	0.23	-0.60	-0.57	-0.60	p_s
p_d	0.53	0.77	-0.53	1	0.93	-0.28	0.93	0.83	-0.10	0.85	0.85	0.86	p_d
Π	0.39	0.73	-0.81	0.93	1	-0.29	0.96	0.82	-0.17	0.85	0.84	0.86	Π
T_s	-0.39	-0.40	0.24	-0.28	-0.29	1	-0.28	-0.39	0.16	-0.29	-0.32	-0.30	T_s
T_d	0.61	0.88	-0.72	0.93	0.96	-0.28	1	0.94	-0.16	0.85	0.87	0.87	T_d
Ω	0.82	0.98	-0.57	0.83	0.82	-0.39	0.94	1	-0.16	0.78	0.83	0.80	Ω
T_a	-0.07	-0.16	0.23	-0.10	-0.17	0.16	-0.16	-0.16	1	-0.12	-0.13	-0.13	T_a
η_{iso}	0.47	0.70	-0.60	0.85	0.85	-0.29	0.85	0.78	-0.12	1	0.99	1	η_{isc}
η_{gt}	0.56	0.77	-0.57	0.85	0.84	-0.32	0.87	0.83	-0.13	0.99	1	1	η_{gt}
η_{tot}	0.51	0.74	-0.60	0.86	0.86	-0.30	0.87	0.80	-0.13	1	1	1	η_{tot}

TABLE II

Winter correlation matrix

extended with the efficiencies presented in the next section in order to show correlations between calculated and measured variables. Looking at the covariance matrices, the most correlated variables are the process gas flow rate, the fuel flow rate, the compressor speed and the discharge temperature for both cases. This is in agreement with the efficiency models introduced in the next section, where further aspects of the correlations are discussed.

III. Efficiency Models

Different efficiencies are considered for the case of gas compressors driven by dual-shaft gas turbines given the measurements introduced previously. In addition, some fitting variables have to be chosen, in order to approximate the efficiencies as a function of measured variables. This choice directly impacts the quality of the fit, since the fitting variables should fully capture the operation of a unit with respect to the considered efficiency.

The estimation of the efficiencies is based on thermodynamic first principles. The simplest efficiency formulation is the isentropic compressor efficiency η_{iso}. This efficiency is defined as the ratio between isentropic work and actual work. W_{iso} is the work needed to compress the gas from the suction pressure p_s to the discharge pressure p_d without losses using the isentropic temperature rise.

$$W_{iso} = \dot{m}_s \cdot c_{p,NG} \cdot T_s \left(\frac{p_d}{p_s}^{\frac{\gamma-1}{\gamma}} - 1 \right) \tag{2}$$

where $c_{p,NG}$ is the specific heat capacity and γ the ratio of specific heats for natural gas. The actual work W_{actual}

accounts for the losses mainly using the measured discharge temperature T_d and is defined in Eq. 3.

$$W_{actual} = \dot{m}_s \cdot c_{p,NG} \cdot (T_d - T_s) \tag{3}$$

The isentropic efficiency of the gas compressor can then be computed using Eq. 4.

$$\eta_{iso} = \frac{W_{iso}}{W_{actual}} \tag{4}$$

η_{iso} is typically plotted as a map against flow number q and pressure ratio $\Pi = \frac{p_d}{p_s}$, which fully captures the operating point of a gas compressor. This is in accordance with the correlations found in the covariance matrix in the previous section. The isentropic efficiency is mostly correlated with pressure ratio, discharge temperature and discharge pressure. The mapping can be defined as

$$f_{iso} : (q_s, \Pi, \vec{\alpha}_{iso}) \rightarrow \eta_{iso} \tag{5}$$

where f_{iso} is the fitting function and $\vec{\alpha}_{iso}$ its parametrization. Note that there is not much difference in considering the isentropic or adiabatic efficiency as it is explained in [7].
Due to the fact that only a limited amount of information is available on the gas turbine side, the gas turbine efficiency is computed from the actual work needed for the gas compression assuming a power balance on the connecting shaft as depicted in Fig. 2. The gas turbine efficiency η_{gt} is defined as the ratio between actual compression work and the theoretical heat release of the combustion [8].

$$\eta_{gt} = \frac{W_{actual}}{W_{fuel}} \tag{6}$$

W_{fuel} depends on the injected fuel flow $\dot{m}_f$ and on the lower heating value LHV of the combustion fuel, which is the same as the gas transported in the pipeline.

$$W_{fuel} = \dot{m}_f \cdot LHV \tag{7}$$

Different η_{gt} map representations can be found in the literature [9]. In the present work, the gas turbine efficiency map is plotted against the ambient temperature T_a and the actual power P_{actual} due to lack of measurements for other representations. Although the rotor speed does not appear in Eq. 6, the measurement covariance matrix shows as expected that the rotor speed is significantly correlated with η_{gt}. This result underlines the validity of the presented assumptions. The gas turbine map can be expressed as

$$f_{gt} : (T_a, P_{actual}, \vec{\alpha}_{gt}) \rightarrow \eta_{gt} \tag{8}$$

where f_{gt} is the fitting function and $\vec{\alpha}_{gt}$ its parametrization. Finally, the combined or total efficiency is directly obtained by multiplication of Eq. 4 with Eq. 6. Therefore, the total efficiency can be expressed as

$$\eta_{tot} = \eta_{iso} \cdot \eta_{gt} = \frac{W_{iso}}{W_{fuel}} \tag{9}$$

The total efficiency can either be represented using the gas compressor operating point or the gas turbine operating point. Further analysis showed that better fitting results could be achieved using the gas compressor operating point representation. Considering the target application of load sharing optimization for compressor stations, it is obvious that these are the preferred fitting variables. For this purpose the fitting function f_{tot} is defined as

$$f_{tot} : (q, \Pi, \vec{\alpha}_{tot}) \rightarrow \eta_{tot} \tag{10}$$

The strengths of the presented models are the simple derivation from first principles which use available measurements and the formulation as work ratios. Typically, the approximations for the efficiency maps f_{iso}, f_{gt} and f_{tot} are chosen to be quadratic functions in the fitting variables (x, y) and linear in the parametrization $\vec{\alpha}$ [7]. For all efficiencies the same model structure is used, as shown in Eq. 11.

$$f\,(x, y, \vec{\alpha}) = \alpha_1 + \alpha_2 x + \alpha_3 y + \alpha_4 x^2 + \alpha_5 xy + \alpha_6 y^2 \tag{11}$$

IV. Algorithm Structure

Before starting with the details of the adaptation algorithm an overview should be given on the structure of the algorithm as illustrated in Fig. 3. Following the illustration, after some measurement filtering the efficiency is calculated and the previous model is evaluated. Given the approximation error, the decision is made whether to keep the previous model parameters or to update the model parameters by triggering the adaptation algorithm. In parallel to this process, the buffer management block takes care of correctly saving and managing the buffer of past measurements. In the following, the most important blocks will be addressed in more detail.

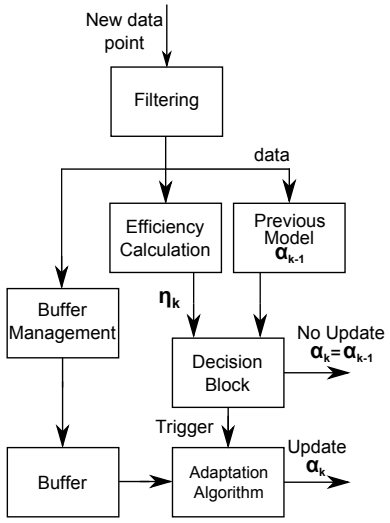

Fig. 3. Function block diagram of proposed algorithm

A. Data Filtering

The main aim of this sub-function is to filter faulty data or data that does not represent normal operation. First it is determined if the compressor is in operation or standby mode, considering a threshold on the compressor speed.
Further filtering is performed using conditions on suction and discharge temperature ratio, as well as on discharge temperature and isentropic temperature rise ratio. These conditions always ensure that the thermodynamic equations are valid

for the considered data point, e.g. ensuring that the discharge temperature is larger than the suction temperature or that the isentropic discharge temperature is smaller than the measured discharge temperature. This might happen only in special cases, typically when the compressor is not connected to the main suction and discharge headers of the compression station. In the case one of the conditions is not fulfilled, the new data point is discarded and not stored.

B. Buffer Management

Data points which were not discarded are stored in a data set subdivided into two parts:

- *global data points*, are stored to keep track of the overall behavior of the system
- *local data points*, represent only the latest data close to the actual operating point

An example of local and global data points for selected time instants are shown in Fig. 4 for the isentropic efficiency and in Fig. 5 for the total efficiency. These figures show the points belonging to the global history in blue circles, whereas the data points contained in the local history are shown as squared black points. It is worth mentioning that 75 data points are shown in the figures and that the contour plot represents the fitted efficiency map. Moreover, these figures give an impression on the spatial extension of global and local data points in the operating range of the gas compressor (shown in black dashed lines).

The local history contains data points which represent the behavior of the compressor in the last N_l observed points. The window length N_l determines how many past observations are stored in this local buffer. If N_l is small, the model will tend towards poor local accuracy and almost invariant global surface shape. Whereas if N_l is large, the model will overfit the local points and the global surface shape will tend to change significantly. Both extreme cases are not desirable. When a new data point has to be stored, all

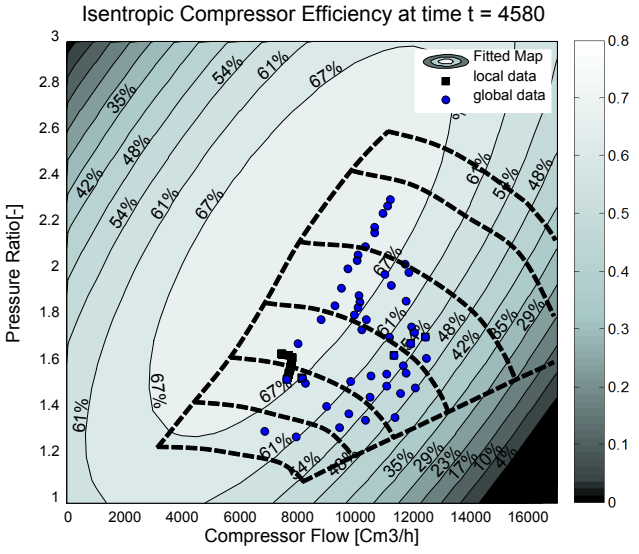

Fig. 4. Snapshot of buffer points and fitted map at a given time instant for the isentropic compressor efficiency. The dashed black lines represent the operating range of the gas compressor

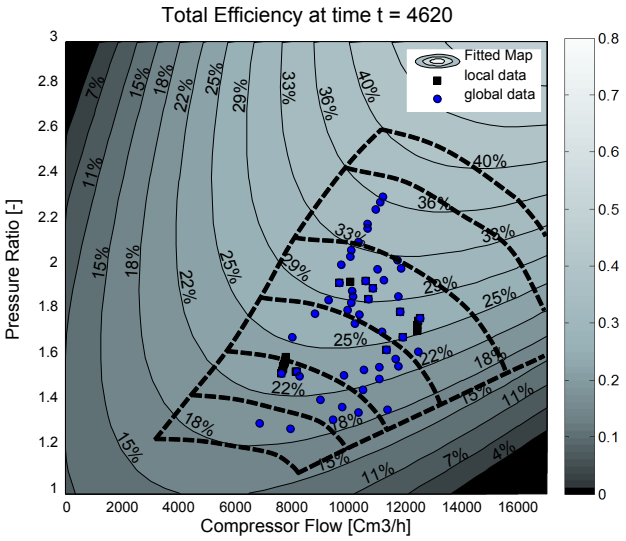

Fig. 5. Snapshot of buffer points and fitted map at a given time instant for the total efficiency. The dashed black lines represent the operating range of the gas compressor

data points are shifted by one in a moving horizon fashion, where the new point takes the first buffer position and the last point drops out of the buffer. This arrangement is also know as First-In-First-Out (FIFO) method. The data point that drops out of the local history is passed to the global history data set.

A global data history was introduced to also account for a larger picture of operating points, which stores the data points that drop out of the local buffer. This buffer is not time-sorted, but rather a list of operating points which were explored recently. If the new data point is in some neighborhood of previously stored points, the older points are replaced by the newly available information. The window N_g is variable but limited by a maximum value. Furthermore, there is a time limitation on how long data points can stay inside the global buffer, e.g. points which are older than one month will be deleted from the buffer automatically.

The distinction between local and global data points is necessary in order to obtain local accuracy and global shape preservation. This solution resulted in a powerful trade-off between overfitting and underfitting. In practice, the distinction between the local and global data points is achieved by means of different weights in the adaptation algorithm using decaying weights for the global data points.

C. Decision Block

The decision block calculates the error between calculated efficiency using the current measurements and by evaluating the efficiency map using the previous map parameters. In the following, the calculated efficiency will be referred to as measured efficiency, whereas the efficiency obtained by map evaluation will be called predicted efficiency. In case the prediction error is too large, the decision block triggers the adaptation algorithm which calculates the new map parameters. This is mainly based on a threshold on the prediction error. To make this approach more robust with respect to outliers, some flexibility is introduced by allowing

temporary violation of the threshold for a limited time. This proved to be a good solution as it will be shown in the results.

D. Adaptation Algorithm

The adaptation is formulated as a least-squares optimization problem with the map parameters serving as decision variables. From now on a generalized notation is used by introducing (x, y) as fitting variables, e.g. (q, Π) or (T_a, P_{actual}) and z as an efficiency calculated using either Eq. 4, Eq. 6 or Eq. 9. The variables x, y and z are normalized before being used in the adaptation algorithm to ensure a good conditioning of the problem and to avoid numerical problems.

$$\min_{\vec{\alpha}} \sum_{i=1}^{N} \omega_i \cdot (z_i - f(x_i, y_i, \vec{\alpha}))^2 \tag{12}$$

where ω_i are the weights and $\vec{\alpha}$ the map parameters. The index i goes over all data points present in the local and global buffer. Using matrix notation the following equation is obtained.

$$\min_{\vec{\alpha}} (\vec{z} - M \cdot \vec{\alpha})^T \cdot W \cdot (\vec{z} - M \cdot \vec{\alpha}) \tag{13}$$

where the matrix W denotes the diagonal weighting matrix and M denotes the measurement matrix which has the following form in case of the selected approximation.

$$M = \begin{bmatrix} 1 & x_1 & y_1 & x_1^2 & x_1 y_1 & y_1^2 \\ \vdots & \vdots & \vdots & \vdots & \vdots & \vdots \\ 1 & x_N & y_N & x_N^2 & x_N y_N & y_N^2 \end{bmatrix} \tag{14}$$

Simplifying Eq. 13 further, the standard quadratic programming (QP) formulation is obtained. Note that the quadratic term in $\vec{z}$ has been dropped, because it is constant in $\vec{\alpha}$.

$$\min_{\vec{\alpha}} \frac{1}{2} \vec{\alpha}^T \underbrace{2 \cdot M^T \cdot W \cdot M}_{H} \vec{\alpha} + \vec{\alpha}^T \underbrace{(-2 \cdot M^T \cdot W \cdot \vec{z})}_{g} \tag{15}$$

In contrast to an analytic least-square solution, the parameters $\vec{\alpha}$ can be constrained by upper and lower bounds. In the present paper the bounds were used to fix the signs of each individual coefficient. This was introduced in order to preserve the shape of the fitted model. Theses bounds were obtained by careful analysis of the data using varying data windows in order to determine common patterns over a whole year. These box constraints are summarized in Eq. 16 and can easily be incorporated in a standard QP formulation. The QP is solved using the active set solver qpOases [10].

$$\begin{aligned} \alpha_1 &\geq 0 & \alpha_3 &\geq 0 & \alpha_5 &\geq 0 \\ \alpha_2 &\leq 0 & \alpha_4 &\leq 0 & \alpha_6 &\leq 0 \end{aligned} \tag{16}$$

Considering the perspective of load sharing optimization the property of having a quadratic function with only one extremum would be a significant advantage. This requirement of being negative definite can be translated into a constraint on the eigenvalues λ_i of the matrix D_i.

$$f = \begin{bmatrix} x \\ y \end{bmatrix}^T \cdot \underbrace{\begin{bmatrix} \alpha_4 & 0.5 \cdot \alpha_5 \\ 0.5 \cdot \alpha_5 & \alpha_6 \end{bmatrix}}_{D_i} \cdot \begin{bmatrix} x \\ y \end{bmatrix} + \begin{bmatrix} x \\ y \end{bmatrix}^T \cdot \begin{bmatrix} \alpha_2 \\ \alpha_3 \end{bmatrix} + \alpha_1$$

The constraint on the eigenvalues of D_i can now be expressed as

$$\underbrace{\alpha_4 + \alpha_6 \pm \sqrt{\alpha_4^2 + \alpha_6^2 - 2 \cdot \alpha_4 \cdot \alpha_6 + \alpha_5^2}}_{\lambda_i} \leq 0 \tag{17}$$

This nonlinear constraint can be reformulated as a quadratic constraint which turns out to be always semi-definite and thus defines a convex feasible set. As the objective function is convex, the resulting convex nonlinear program (NLP) can be solved either by a dedicated quadratically constrained QP (QCQP) algorithm or by means of a general semidefinite programming (SDP) solver. Yet another alternative is to iteratively linearize the nonlinear constraint and to solve several standard QPs in an SQP-type fashion. Numerical tests indicate that this sequential QP (SQP) approach converges to the solution of the convex NLP within a very small number of iterations. Summarizing, in case the original QP solution is not negative definite, the constraints on the bounds are removed and replaced by iteratively linearizing the nonlinear constraint on the eigenvalues as illustrated in Fig. 6. The presented method uses only a QP solver and can therefore be easily implemented in an embedded environment.

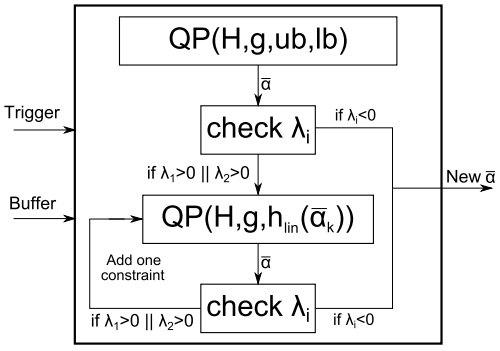

Fig. 6. Details of the adaptation algorithm using only QP formulations

V. Results

A data set corresponding to a time period of approximately 40 days was selected from the compressor station historical database to demonstrate the performance of the proposed algorithm. The results are shown for only one compressor due to space reasons. The statistics at the end of this section include all five compressors. First, the trends for calculated and predicted isentropic compressor efficiency are shown in Fig. 7. The error evolution stays quite tight inside the band up to data point 4550. After an error of approximately 8% the model parameters are updated and the model performance returns inside the error band. In total only two parameter updates are triggered during the considered period. Despite significant variations in the efficiency between the data points 4600 and 4800 coming from highly variable operating points, the model continues to perform very well. Moreover, the efficiency prediction is accurate also before and after the compressor shut down between 4200 and 4300. Similar trends can be observed for the gas turbine efficiency in Fig. 8. Also for this efficiency only two updates were triggered in the considered time period. The influence of the robust

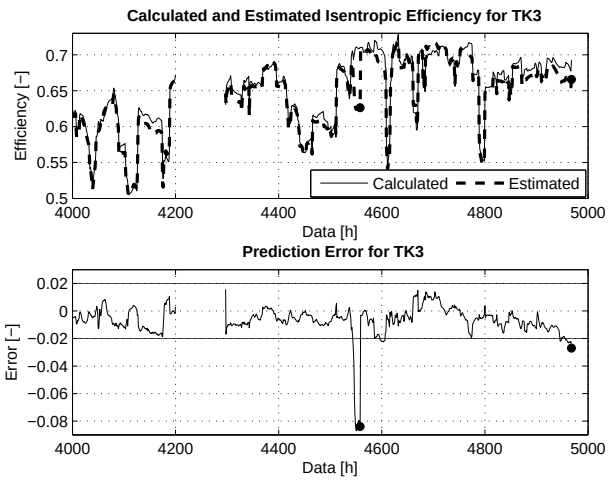

Fig. 7. Calculated and estimated isentropic compressor efficiency. Black points indicate an update of model parameters

decision part of the algorithm can be seen at points 4600 and 4800, where the error band is violated but only for a very limited time period. The algorithm does not update the model parameters and the model performs well after the temporary violation. This proved to be a powerful solution to avoid unnecessary and excessive parameter updates. Finally, the

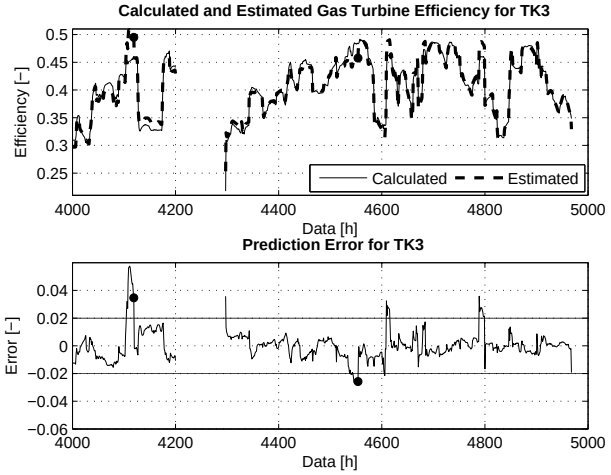

Fig. 8. Calculated and estimated gas turbine efficiency. Black points indicate an update of model parameters

total efficiency evolution is depicted in Fig. 9. For this case three parameter updates are observed all in the neighborhood of data point 4550. Nevertheless, the model performance is accurate throughout the data set. The only difference is the higher variability of the error inside the error band.

As additional information the computational time needed to solve the problem, the statistics of model updates and parameter variations are given in the following. The mean execution times were $1.84ms$ for the QP problems and $26.42ms$ for the SQP. To capture the statistics on model updates the ratio R between number of model updates and working hours in the year is introduced. Averaging over one year and over the different compressors the following statistics were obtained.

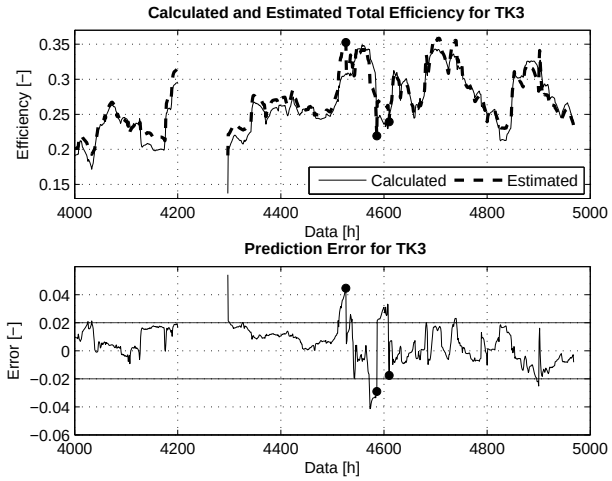

Fig. 9. Calculated and estimated total efficiency. Black points indicate an update of model parameters

$$\mu(R) = \frac{1}{244} = 0.0041 \qquad \sigma(R) = 1.5 \cdot 10^{-6} \tag{18}$$

This means that in average there is one map update every 244 working hours, which corresponds to approximately 10 working days. The small standard deviation shows that similar update behavior is observed for all efficiency definitions.

VI. Conclusion

An adaptation algorithm for centrifugal compressors is presented accounting for different efficiency definitions in the case of variable-speed gas turbine driven gas compressors. The map adaptation is formulated as an optimization problem using historical data buffering and is solved as QP and SQP in order to enforce a concave fitting. The results obtained using industrial data from a compression station, show that the proposed algorithm is accurate and avoids excessive parameter updates. The data underline also the fact that a map adaptation is necessary in order to be able to accurately predict the evolution of different efficiencies over time. The presented method can be used for various purposes including compressor load sharing optimization.

References

[1] R. Kurz, K. Brun and M. Lubomirsky *Gas compressor station economic optimization*. Int. Journal of Rotating Machinery, 2011.

[2] F. Paparella, L. Dominguez, A. Cortinovis, M. Mercangöz, D. Pareschi, S. Bittanti *Load sharing optimization of parallel compressors*. ECC Conference Zürich, 2013.

[3] M. N. Saxena. *Optimize gas turbine-driven centrifugal compressors*. Hydrocarbon processing, 11:61–64, 2000.

[4] J. Petek, P. Hamilton *Performance Monitoring For Gas Turbines*. Journal of Orbit, 25(1):6474, 2005.

[5] American Society of Mechanical Engineers *Performance Test Code on Compressors and Exhausters*. A. S. M. E. Press, 1998.

[6] K.B. Ariyur, M. Krstic. *Real-Time Optimization by Extremum Seeking Feedback*. Wiley Interscience, 2003.

[7] B. D. Rasmussen, A. Jakobsen *Review of Compressor Models and Performance*. International Compressor Engineering Conference. Paper 1429, 2000.

[8] M. P. Boyce *Gas Turbine Engineering Handbook*. 2nd ed., Elsevier Science, Houston, 2002.

[9] R. Kurz, K. Brun *Gas Turbine Performance - What Makes The Map?* Proceedings of the 29th Turbomachinery Symposium, 2000.

[10] H. J. Ferreau, H. G. Bock and M. Diehl *An online active set strategy to overcome the limitations of explicit MPC*. International Journal of Robust and Nonlinear Control, vol. 18, no. 8, 2008.